Non-Enzymatic and Highly Sensitive Lactose Detection Utilizing Graphene Field-Effect Transistors

Eric Danielson*[1], Mirco Dindo[2], Alexander J. Porkovich[1], Pawan Kumar[1], Zhenwei Wang[1], Prashant Jain[3], Trimbak Mete[3], Zakaria Ziadi[1], Raghavendra Kikkeri[3], Paola Laurino[2], Mukhles Sowwan[1]

[1]Nanoparticles by Design Unit, Okinawa Institute of Science and Technology (OIST) Graduate University, 1919-1 Tancha, Onna-Son, Okinawa 904-0495, Japan

[2]Protein Engineering and Evolution Unit, Okinawa Institute of Science and Technology (OIST) Graduate University, 1919-1 Tancha, Onna-Son, Okinawa 904-0495, Japan

[3]Indian Institute of Science Education and Research, Dr. Homi Bhabha Road, Pune, 411008, India.

S1. Graphene Field-Effect Transistor Fabrication & Graphene Characterization

Graphene was synthesized in a CVD system (Easytube 2000, FirstNano, USA) on a 30 µm thick commercial copper foil (Nilaco, Japan). After sonication in acetone and isopropyl alcohol (IPA), the copper foil was first annealed for 1 hour at 990 °C at 760 torr, with a gas mixture of Ar and H_2 at flow rates of 4875 and 125 standard cubic centimeter per minute (sccm), respectively. The graphene growth step was performed for 15 min at 1000 °C at 760 torr, with a gas mixture of Ar, H_2, and CH_4 with flow rates of 4875, 125, and 2.5 sccm, respectively. The sample was then cooled to room temperature under an Ar flow rate of 5000 sccm.

Graphene transfer from the copper foil to Si:SiO_2 substrates was performed using a Poly(vinyl alcohol) (PVA) lamination method (Shivayogimath et al., 2019). PVA films (Cubic Coating) were rinsed in IPA and dried with N_2, while the copper foil pieces with CVD grown graphene were placed in deionized (DI) water for 8 hours to facilitate the intercalation of graphene from the Cu or Cu_2O surface(Wu et al., 2016). After drying, the PVA film and the graphene covered copper foil were laminated together at 110 °C and a speed of 15 mm/s using a commercial laminator (Meiko Shokai THS 330). The laminate was baked on a hot plate at 110 °C for 1 min to improve the PVA/graphene adhesion. Peeling the PVA film off the copper foil removes the graphene as well. The graphene on PVA can be transferred to the desired Si:SiO_2 substrates using a second lamination step with the same conditions. After baking at 110 °C for 1 min, the paper support of the PVA film is peeled off while the sample is still on the hot plate. Placing the sample in room temperature water overnight dissolves the PVA layer, leaving a monolayer graphene layer on top of the target substrate.

Si:SiO_2 substrates (oxide thickness of 300 nm) covered with monolayer graphene were patterned into biosensor devices using a maskless lithography system (Dlight DL-1000GS/OIC) and oxygen plasma etching for 1 min at 100 W. Ti/Au contacts (5/50 nm) were deposited by e-beam evaporation and defined using photolithography. After lift-off of the metal contacts and cleaning in acetone and IPA, the samples were placed in 1-methyl-2-pyrrolidone (NMP) for 4 hours to remove residual photoresist from the graphene surface.

Raman spectrum of graphene on Si:SiO_2 was obtained using a 3D Laser Raman Microspectrometer Nanofinder 30 (Tokyo Instruments) with 532 nm excitation and a 600 l/mm resolution.

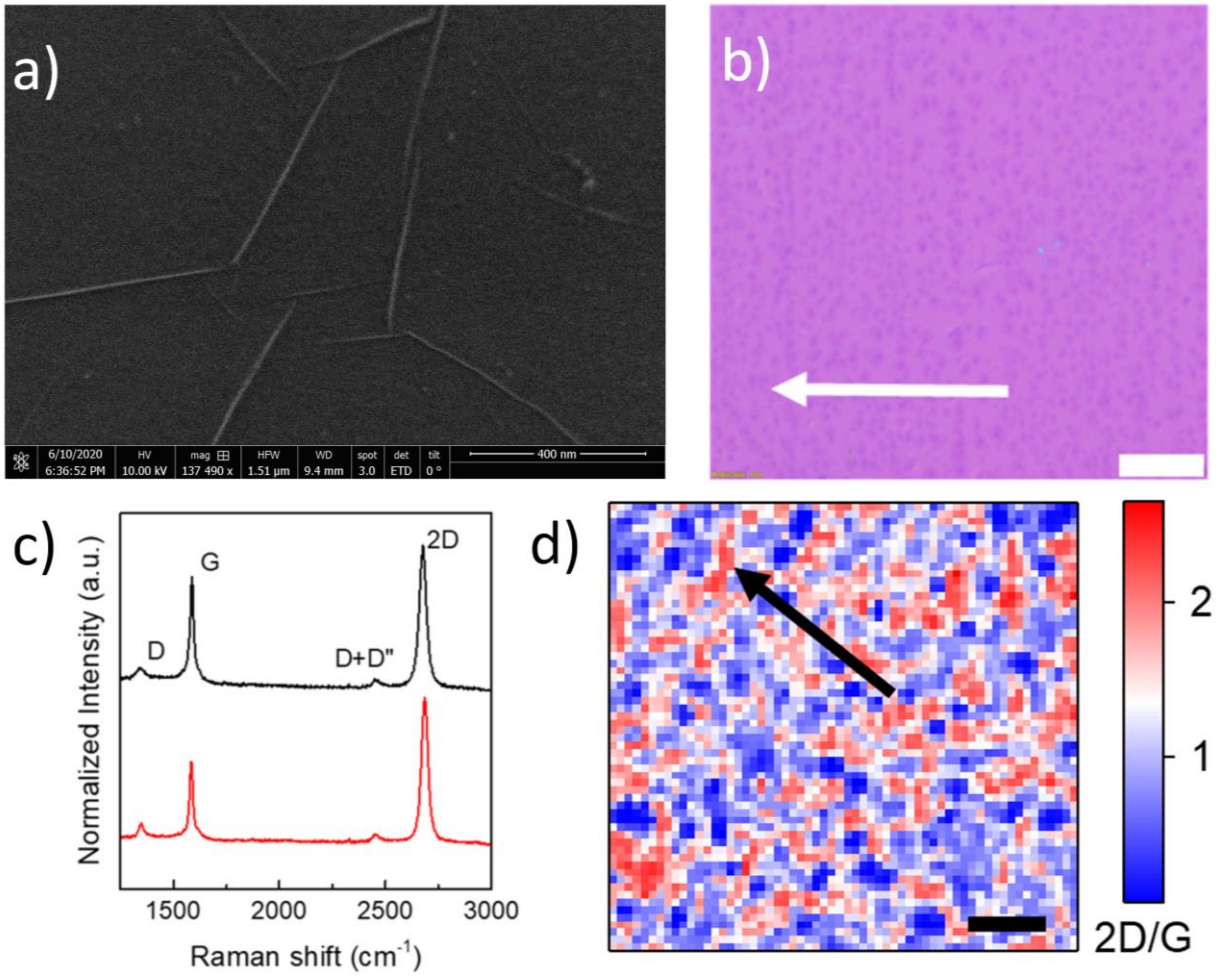

Fig. S1: Laminated Graphene Quality. (a) SEM image of monolayer graphene on Si:SiO_2 **(b)** Microscope image of graphene on SiO_2/Si substrate. The scale is 10 µm and the arrow represents the peeling direction. **(c)** Typical Raman spectra of transferred graphene from the dark (top black line) and light-colored (bottom red line) zones in (b). **(d)** 2D/G peak height ratio of the transferred graphene from Raman mapping measurement. The scale bar is 5 µm and the arrow represents the peeling direction.

A typical scanning electron microscope (SEM) image of the transferred graphene is shown in **Fig. S1a**, with individual discontinuities in the monolayer film visible at the sub-micron scale. A light microscope image of the transferred graphene is shown in **Fig. S1b**, with small with small regions of dark purple distributed over a lighter coloured background. The darker zones, which suggest areas of thicker graphene (No et al., 2018), are arranged in a line style normal to the direction of laminate peeling. The linear arrangement is possible due to the stress accumulation during the peeling process. In spectra from both the light and dark coloured areas in **Fig. S1c**, the typical Raman peaks of G (ca. 1590 cm^{-1})

and 2D (ca. 2680 cm^{-1}) peaks are prominent, while the D (ca. 1590 cm^{-1}) and D+D" (ca. 2450 cm^{-1}) peaks are also observed, which indicate the presence of grain boundaries, surface contamination, or other defects, are much smaller. Both peaks are quite low and comparable to previous reports; indicating a low defect density in the transferred graphene (Afsahi et al., 2018; Campos et al., 2018; Roscher et al., 2019).

The 2D/G peak height ratio can be used for estimating the thickness of graphene: 2 for monolayer and 1 for bilayer graphene (Graf et al., 2007). Peak height ratios for the dark and light-colored zones were 1.42 and 1.9, respectively. Deviation of the 2D/G ratio from the ideal value of 2.0 is due to the relatively large Raman laser spots, so that signals from both zones would inevitably be collected. The same theory also explains the value of 1.42 for the darker zones, as the height ratio should be ca. 1.0 for bilayer graphene. A Raman mapping image illustrating the 2D/G height ratio distribution is shown in **Figure S1d**, in which regions of low ratio (blue) interspersed with regions of high 2G/D (red). This observation from Raman mapping agrees with the optical microscope measurements that the laminate transferred graphene consists of an overall monolayer with isolated islands of bilayer graphene.

The Au NP decorated G-FETs were electrically characterized using liquid gate measurements. Due to the electronic band structure of graphene, the source-drain current flow I_d of a G-FET cannot be switched off at room temperature. However, the type of charge carrier flowing in the graphene channel at an applied drain voltage V_d can be tuned from holes to electrons by applying an external gate voltage V_g. In a liquid gate configuration, the V_g is applied using a reference electrode immersed in a solution exposed to the graphene channel. At the transition between the electron and hole regime, the current is minimized at a specific V_g, the charge neutrality point V_{CNP}. The V_{CNP} of G-FETs can be tuned by either the electrostatic gating or doping from molecules bound to the graphene surface. Thus, the shift in V_{CNP} caused by analyte binding can be used as the sensor response for a G-FET.

S2. Gold Nanoparticle (Au NP) Decoration

Nanoparticles were deposited using the magnetron assisted gas aggregation method (Steinhauer et al., 2015; Grammatikopoulos et al., 2016; Datta et al., 2019; Porkovich et al., 2019; Vernieres et al., 2019). This consists of two connected chambers (the aggregation and deposition chambers) held to different gas pressures. A high purity (99% Kurt J Lesker) Au target was bombarded with an Ar plasma, freeing Au atoms for nanocluster formation in the higher-pressure aggregation chamber. Nanoparticle size and crystallinity were controlled by adjusting the plasma power, the physical distance of the magnetron/target to the end of the chamber, the pressure difference between the aggregation chamber and the deposition chamber where the samples are placed, and by a quadrupole mass filter (QMF) between the two chambers. The base pressure in the deposition chamber and aggregation zone before deposition was maintained below $\sim 1.5 \times 10^{-7}$ and $\sim 2.5 \times 10^{-6}$ mbar, whereas the process pressures were $\sim 1.4 \times 10^{-3}$ and $\sim 4.5 \times 10^{-1}$ mbar, respectively. Depositions were performed using an Ar flow rate of 100 sccm, a DC power of ~6 W, and an aggregation zone length of 125 mm. The substrate holder was rotated at 2 rpm to ensure uniform NP decorating density.

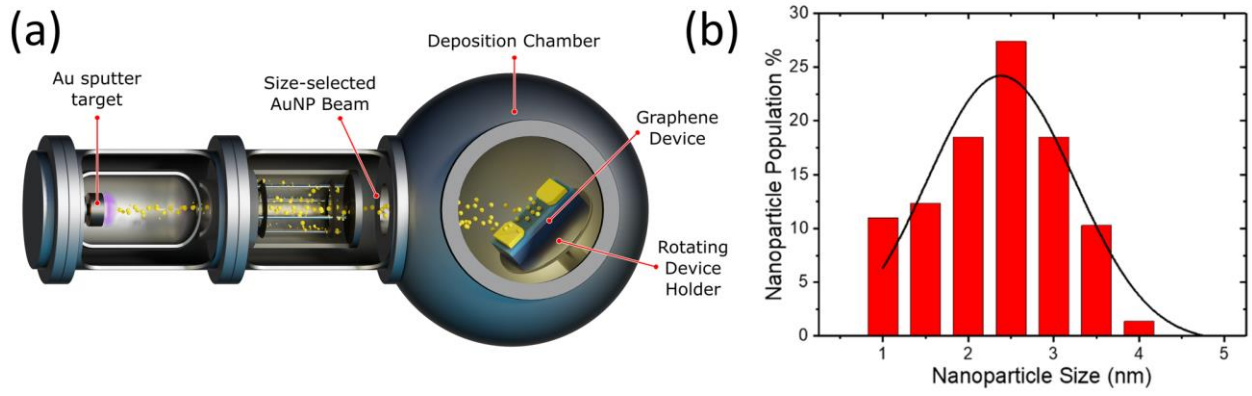

Fig. S2: Gas-Phase Synthesis of Au NPs. (a) Schematic diagram of the magnetron sputtering inert gas condensing system for synthesis and size selection of the Au NPs. **(b)** Particle size histogram (red) of sputtered Au NPs on a Si3N4 TEM grid. Particle diameter was measured and fitted with a Gaussian curve (black). *Reproduced with permission from (Danielson et al., 2019).*

S3. CRD hGal-3 and hGal-3 M249C Purity

HGal-3 is a small soluble protein of 28 kDa belonging to the S-type lectin family, which is found expressed inside mammalian cells and also secreted into circulation (Barondes et al., 1994; Kasai et al., 1996). HGal-3 plays a key role in several intracellular physiological and pathological processes including proliferation and apoptosis (Lis et al., 1998; MacKinnon et al., 2008). In addition, hGal-3 is involved in extracellular cell-cell interaction and inflammatory processes through native neutrophile activation (Liu et al., 2010; Johannes et al., 2018).

DNA encoding amino acids 113-250 of the human galectin-3 (hGal-3) gene (carbohydrate binding domain CRD) with the 6x His-tag and the thrombin recognition sequence at the C-terminus was amplified *via* polymerase chain reaction from hGal-3 in pET3C (Massa et al., 1993) and cloned into the pET28a vector using NcoI and BamHI (New England Biolab) restriction enzymes. The plasmid containing the gene for the CRD domain of hGal-3 was used as a template for the generation of the variant M249C using Q5 mutagenesis kit (New England Biolab) (Mutagenic primers: 5'-CTTCATATACCTGTATACATCATCATCACC-3', 3'-CACTGGTGAGGTCTATG-5', the mutated codon is underlined). The presence of the mutation has been confirmed by sequencing. E. coli BL21 cells transformed with the constructs encoding the CRD domain or the CRD domain M249C were grown in 1 L of Luria broth at 37 °C to an absorbance at 600 nm of 0.4-0.6 in the presence of 50 µg/mL Kanamycin. The expression was induced with 0.4 mM IPTG for 15 hours at 25 °C. Cells were harvested and resuspended in 20 mM sodium phosphate buffer, pH 7.4, containing 0.5 M NaCl and 20 mM imidazole supplemented with benzonase (Novagen) at a dilution of 10^4 - 10^5, Lysozyme 0.2 mg/mL and protease inhibitor cocktail for purification of His-tagged proteins. After a freeze-thaw, the lysate was centrifuged at 30,000 g for 30 min at 4 °C. The lysate was loaded on a Nickel beads equilibrated with 20 mM sodium phosphate buffer, pH 7.4, containing 0.5 M NaCl and 20 mM imidazole. The proteins have been eluted by using two different elution buffers (20 mM sodium phosphate buffer and 0.5 M NaCl, pH 7.4) containing 100 and 500 mM imidazole. The fraction obtained from the elution buffer

containing 500 mM imidazole was concentrated and extensively dyalized against 0.01x PBS buffer, pH 7.4, using Amicon Ultra 15 concentrators (3 KDa cutoff) and then stored at -20 °C. The His-Tag at the C-terminus of the CRD WT was cut following the procedures previously reported in (Hefti et al., 2001). Protein concentration was determined by using the predicted molar absorption coefficient (https://web.expasy.org/protparam/) of 9970 M^{-1} cm^{-1} at 280 nm (Gasteiger et al., 2005) using a Shimadzu UV-1900 Spectrophotometer (Shimadzu, Kyoto, Japan).

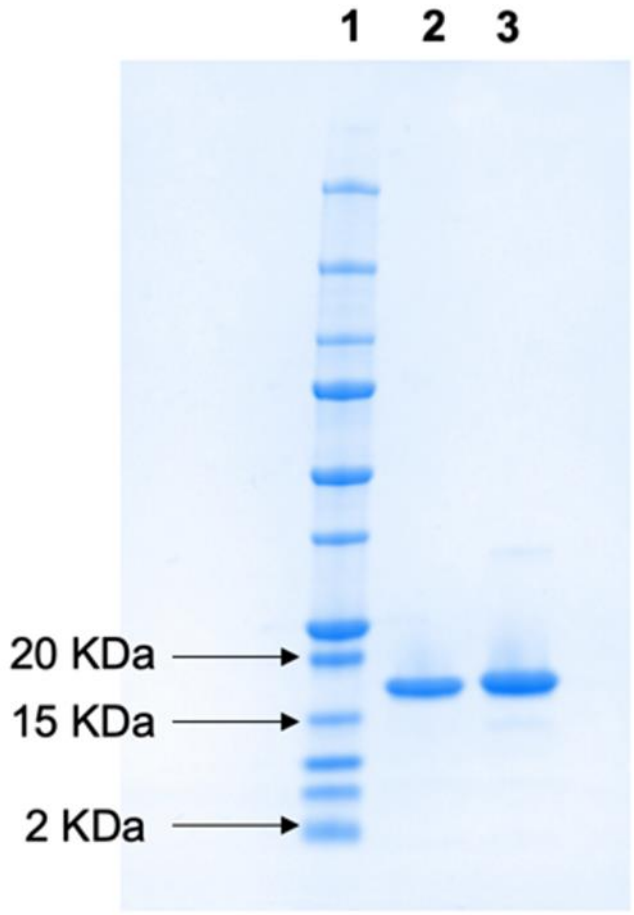

Fig. S3: SDS-PAGE of CRD Wildtype (WT) and the Mutant M249C After Purification. 1= Molecular weight marker, 2= CRD hGal-3 WT, 3= CRD hGal-3 M249C mutant.

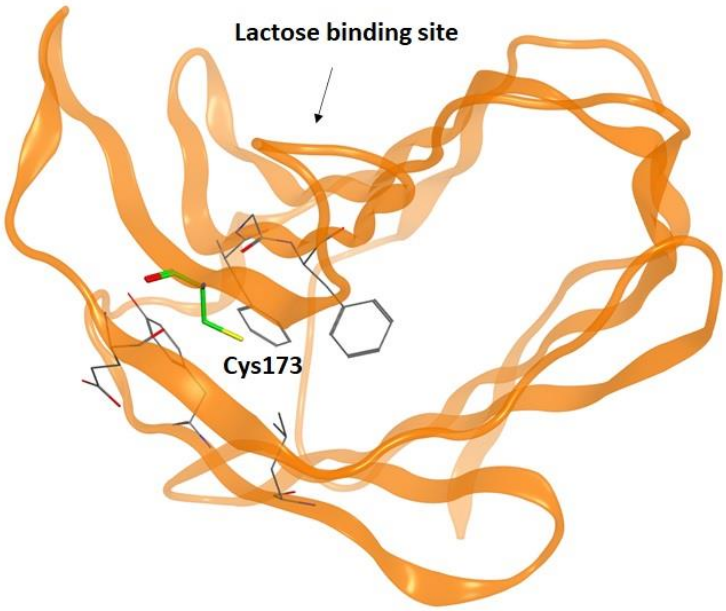

Fig. S4: Position of the Residue Cys173 in the Crystal Structure of hGal-3 CRD. The Cys173 is highlighted as a green stick and the neighbouring residues as a grey stick.

S4. I_d-V_g Sensing Control Experiments

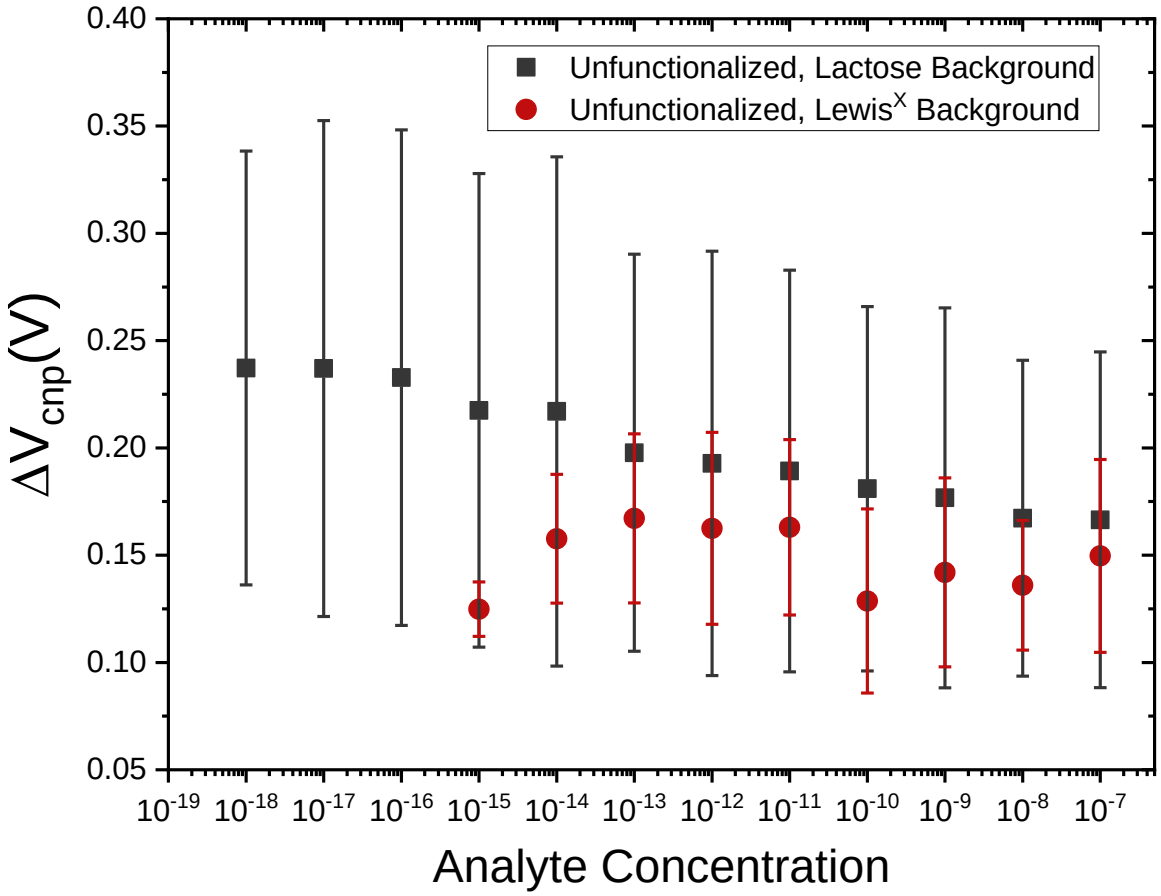

Fig. S5: G-FET Sensor Response Without hGal-3. The shift of V_{CNP} for bare G-FET biosensors exposed to solutions of lactose or Lewis^X in 0.01xPBS. Error bars indicate standard deviations from measurements with n = 5.

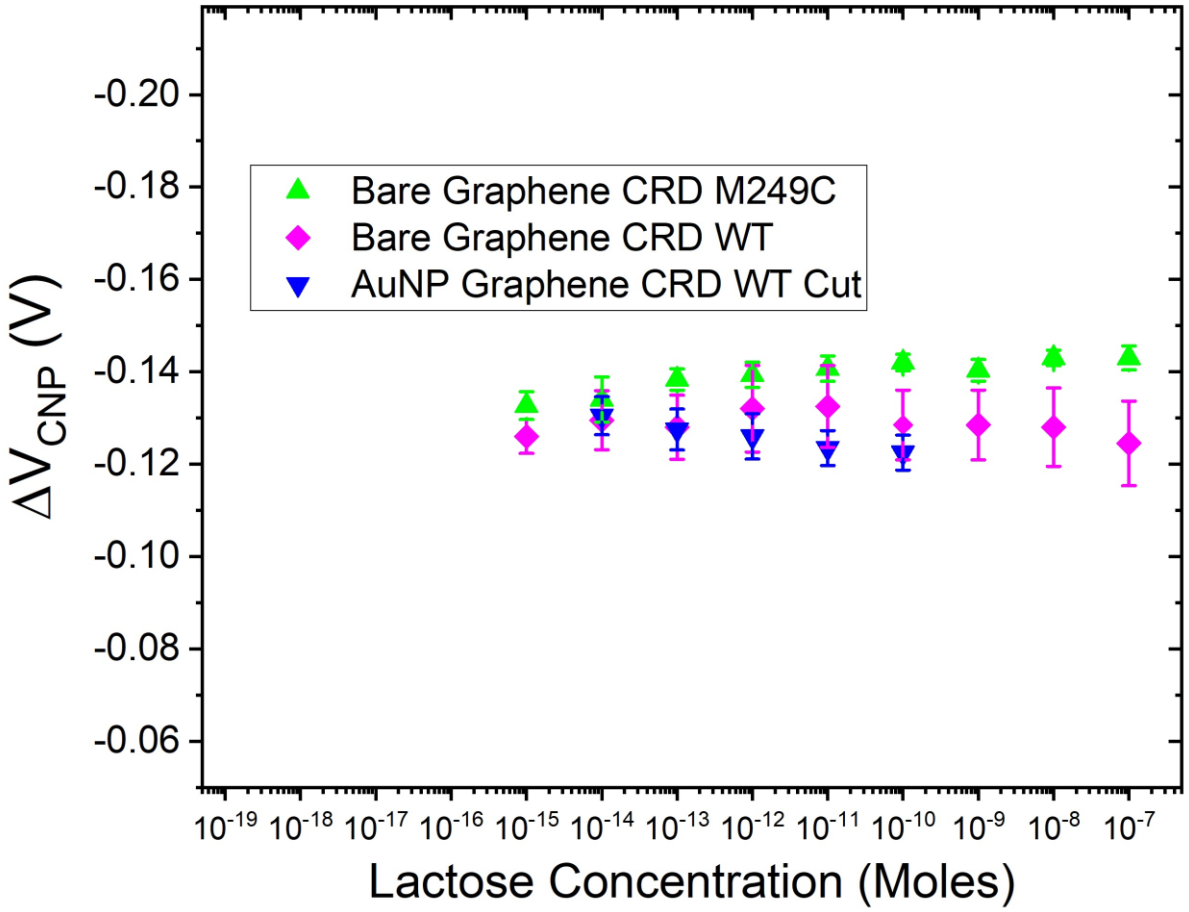

Fig. S6: G-FET Sensor Control Experiments. The shift of V_{CNP} for G-FET biosensors functionalized with different engineered proteins after exposure to various concentrations of lactose, presented at the same scale as **Fig. 5** in the main text. Error bars indicate standard deviations from measurements with n = 5.

Table S1. Literature Survey of Lactose Sensor Characteristics

Work	LoD (M)	Range (M)	Sensing Conditions	Sensing Mechanism	Device
(Rajendran et al., 2002)	0.2 x 10^{-3}	0.2 – 20 x 10^{-3}	0.1xPBS (pH 7.0)	Electrochemical	GOx-β-Gal[a] @ Pt electrode
(Yakovleva et al., 2012)	0.05 x 10^{-3}	0.1 – 50 x 10^{-3}	1:150 Diluted Milk	Thermometric / Electrochemical	CDH[b] @ controlled pore glass
(Tasca et al., 2013)	0.5 x 10^{-6}	1 – 150 x 10^{-6}	0.1 M acetate buffer (pH 3.5)	Electrochemical	PsCDH NH_2-PD[c]/SWCNT[d] @ Glassy Carbon electrode
(Nguyen et al., 2016)	3.79 x 10^{-6}	29.2 – 175.2 x 10^{-6}	Lactose Model Solution (pH 7.0)	Electrochemical	GOx-β-Gal@ Pt / graphene / 1,5-polydiaminonaphthalene
(Lopez et al., 2017)	10 x 10^{-6}	10 – 4500 x 10^{-6}	1xPBS (pH 7.0)	Electrochemical	rec-CtCDH / PDADMAC[e] @ graphite electrode
(Çakıroğlu et al., 2019)	0.23 x 10^{-6}	0.008 – 2.50 x 10^{-3}	0.1xPBS (pH 7.0)	Photoelectrochemical	GOx-β-Gal@ Au NPs-g-C_3N_4-MnO_2 @ TiO_2/ITO electrode
(Han et al., 2019)	58 x 10^{-3}	58 – 81 x 10^{-3}	Lactose Model Solution (pH 7.0)	Terahertz Spectroscopy	Cu on Quartz Substrate
This Work	200 x 10^{-18}	1 – 100 x 10^{-15}	0.01xPBS (pH 7.4)	Field-Effect	Graphene with mutant hGal-3 attached via Au NPs

[a]Glucose oxidase and β-galactosidase

[b]Cellobiose Dehydrogenase (CDH)

[c]P-phenylenediamine

[d]Single walled carbon nanotube

[e]Poly(diallyldimethylammonium chloride)

Table S2: G-FET Sensor Selectivity. The average shift in V_{CNP} for Au NPs decorated G-FET devices (n = 5) after exposure to various concentrations of different carbohydrates in 0.01x PBS. Numbers in parentheses indicate relative standard deviation (%).

Analyte	ΔV_{CNP} (mV) @ 100 aM	ΔV_{CNP} (mV) @ 100 fM	ΔV_{CNP} (mV) @ 100 pM	ΔV_{CNP} (mV) @ 100 nM
Lactose	– 137 (5.2)	– 171 (4.9)	– 189 (3.2)	– 195 (2.2)
Glucose	88 (3.6)	91 (4.7)	85 (2.1)	78 (9.4)
Mannose	104 (24.6)	99 (21.5)	87 (26.0)	87 (27.5)
Sucrose	69 (3.0)	74 (2.3)	75 (2.0)	76 (2.6)
$Lewis^X$	– 80 (1.8)	– 88 (2.3)	– 96 (1.5)	– 116 (4.3)

S5. Synthesis of Lewis^X trisaccharide

All chemicals were reagent grade and used as supplied except where noted. Analytical thin layer chromatography (TLC) was performed on Merck silica gel 60 F254 plates. Compounds were visualized by UV irradiation or dipping the plate in CAM/ninhydrin solution followed by heating. Column chromatography was carried out using force flow of the indicated solvent on Fluka Kieselgel 60 (230–400 mesh). ^{1}H and ^{13}C NMR spectra of all compounds were recorded on Jeol 400 MHz, and Bruker 600 MHz with cryo probe using residual solvents signals as an internal reference ($CDCl_3$ δH, 7.26 ppm, δC 77.3 ppm, CD_3OD δH 3.31 ppm, δC 49.0 ppm and D_2O δH 4.79 ppm). The chemical shifts (δ) are reported in ppm and coupling constants (J) in Hz.

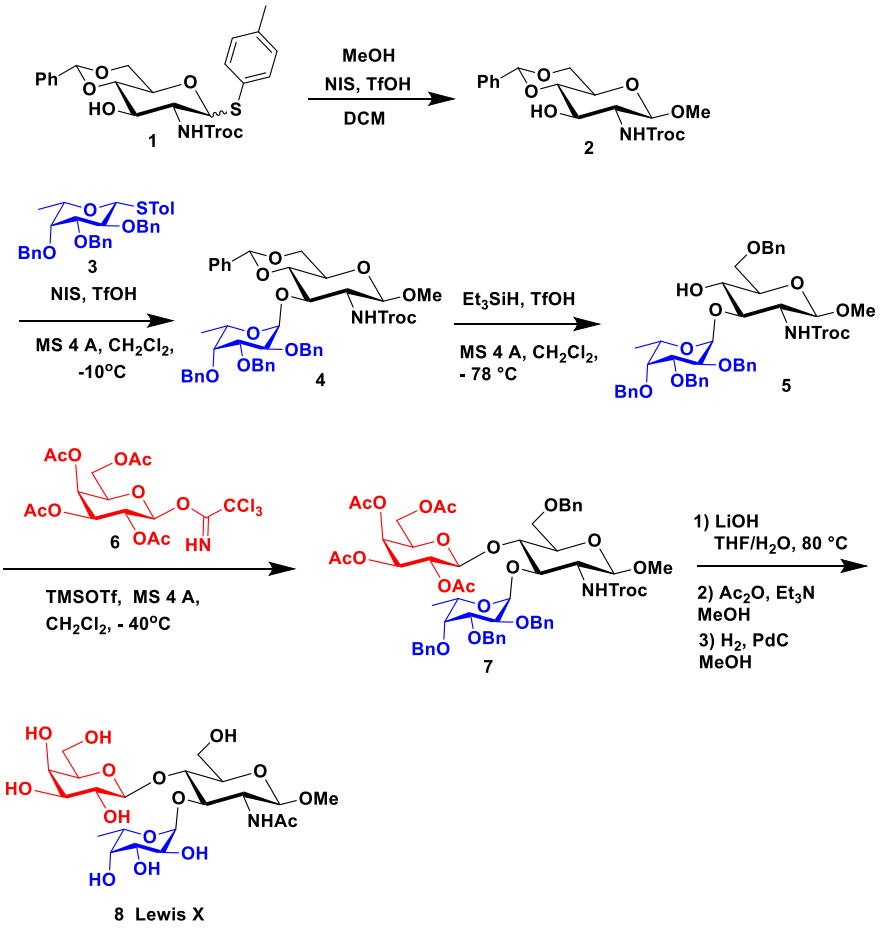

Fig. S7: Synthesis of Lewis^X Trisaccharide Methyl Glucoside.

Synthesis and NMR Spectra of Compound 2

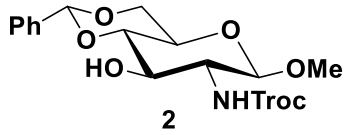

A solution of **1** (500 mg, 0.910 mmol, 1.0 equiv) and methanol (146 *µl*, 4.55 mmol, 5 equiv) in anhydrous dichloromethane (10 ml) was stirred for 10 min at 0 °C under N_2 atmosphere, and then added NIS (246 mg, 1.09 mmol, 1.2 equiv) and TfOH (32 *µl*, 0.364 mmol, 0.4 equiv). The reaction mixture was stirred at 0 °C for 30 min until the disappearance of the donor on TLC, then quenched with triethylamine and warmed to room temperature. The mixture was diluted with dichloromethane, washed with 20% aqueous $Na_2S_2O_3$ solution, dried over Na_2SO_4, and concentrated under reduced pressure. The residue was purified by column chromatography on silica gel to afford the compound **2** as white solid (403 mg, 97 %).

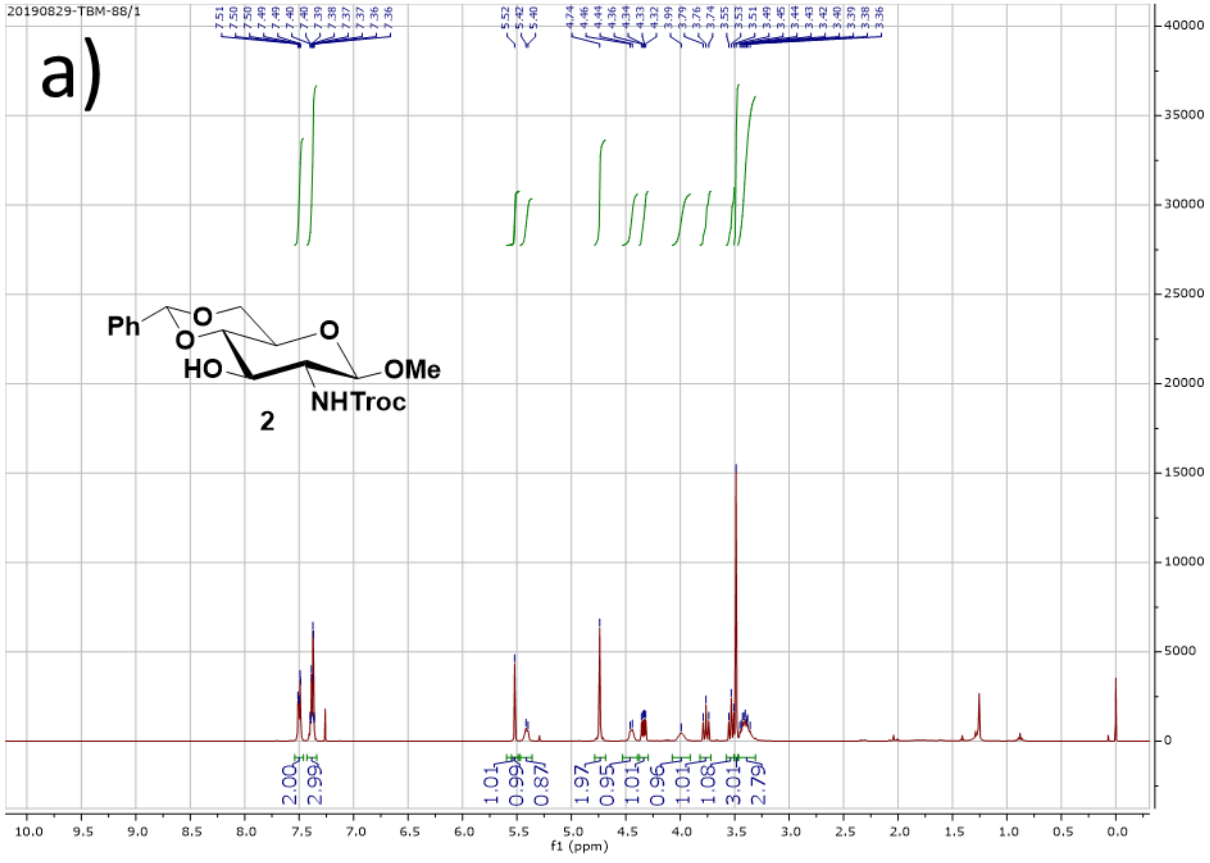

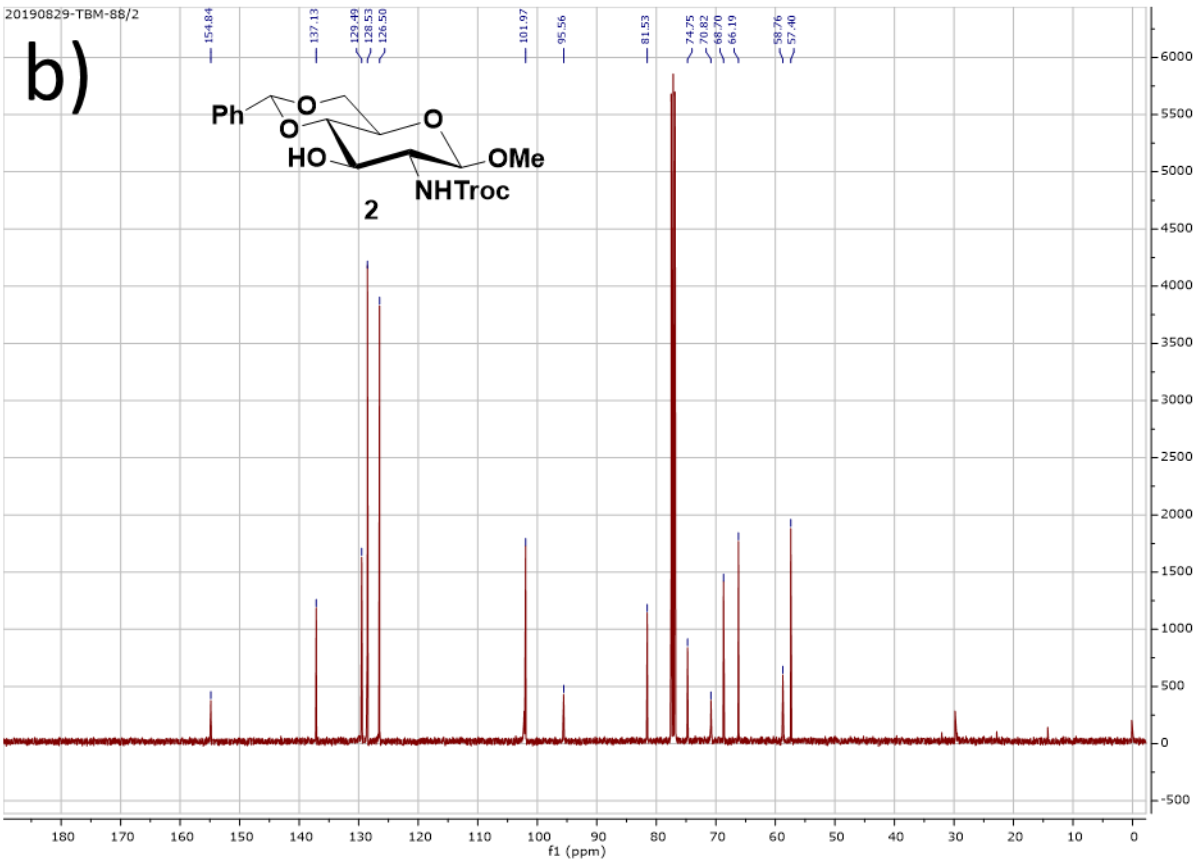

Fig. S8: NMR Spectra of Compound 2. ^{1}H **(a)** and ^{13}C **(b)** NMR spectra. (β-Isomer) ^{1}H NMR (400 MHz, Chloroform-*d*) δ 7.51 – 7.49 (m, 2H), 7.40 – 7.36 (m, 3H), 5.52 (s, 1H), 5.41 (d, *J* = 7.6 Hz, 1H), 4.74 (s, 2H), 4.45 (d, *J* = 8.1 Hz, 1H), 4.34 (dd, *J* = 10.5, 5.0 Hz, 1H), 3.99 (s, 1H), 3.76 (t, *J* = 10.3 Hz, 1H), 3.53 (t, *J* = 9.2 Hz, 1H), 3.49 (s, 3H), 3.45 – 3.36 (m, 3H). ^{13}C NMR (100 MHz, Chloroform-*d*) δ 154.8, 137.1, 129.5, 128.5, 126.5, 102.0, 95.6, 81.5, 74.8, 70.9, 68.7, 66.2, 58.8, 57.4. HRMS (ESI) calcd. for $C_{17}H_{20}Cl_3NO_7$ $[M + H]^+$ 456.0384, found 456.0381.

Synthesis and NMR Spectra of Compound 4

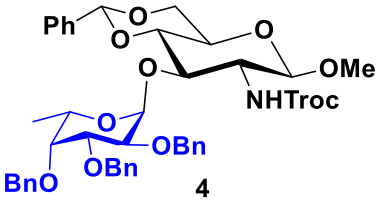

A solution of **2** (400 mg, 0.875 mmol, 1.0 equiv), fucose donor **3** (439 mg, 1.05 mmol, 1.2 equiv), and activated 4Å powdered molecular sieves (0.5 g) in anhydrous dichloromethane (8 ml) was stirred for 2 hours at room temperature under N_2 atmosphere, and then cooled to 0 °C followed by addition of NIS (296 mg, 1.31 mmol, 1.5 equiv) and TfOH (31 *µl*, O.350 mmol, 0.4 equiv). The reaction mixture was stirred at -10 °C for 30 min until the disappearance of the donor on TLC, then quenched with triethylamine and warmed to room temperature. The mixture was diluted with dichloromethane, filtered through celite, washed with 20% aqueous $Na_2S_2O_3$ solution, dried over Na_2SO_4, and concentrated under reduced pressure. The residue was purified by column chromatography on silica gel to afford the compound **4** (591 mg, 77 %).

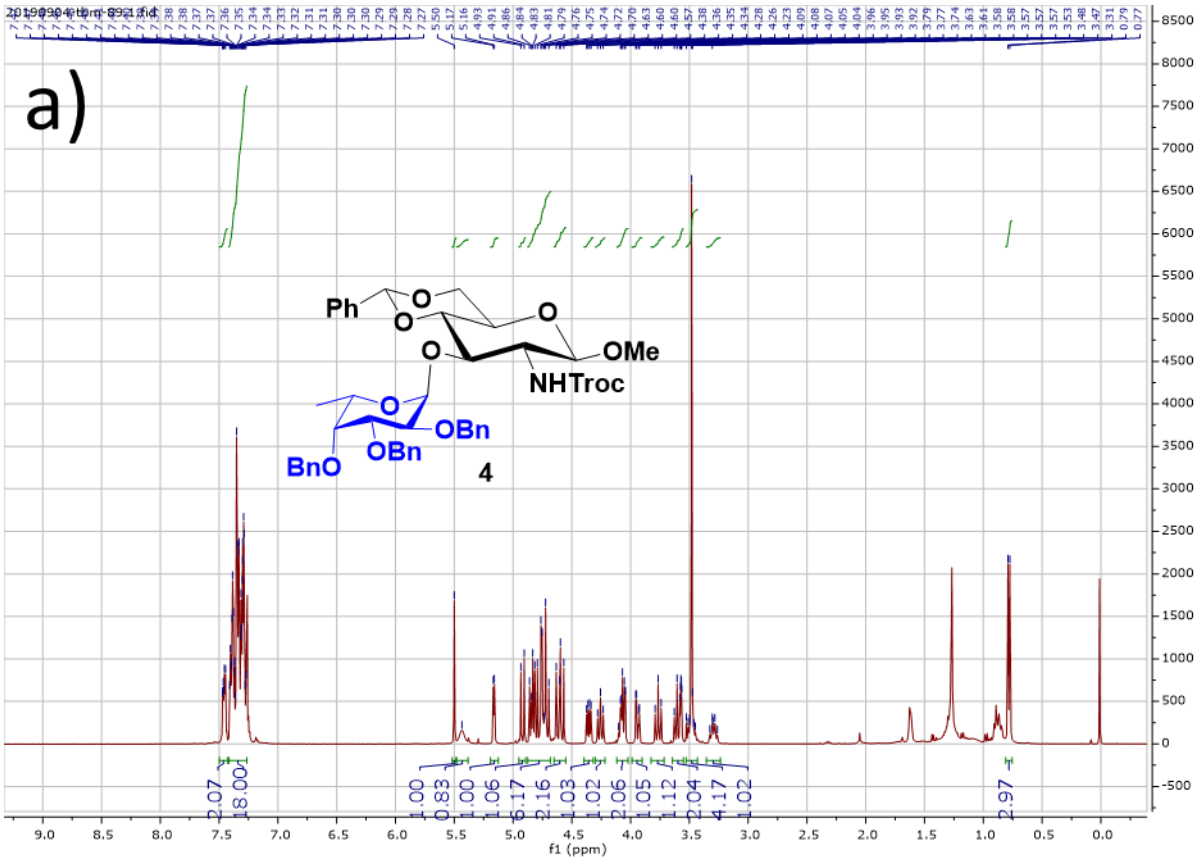

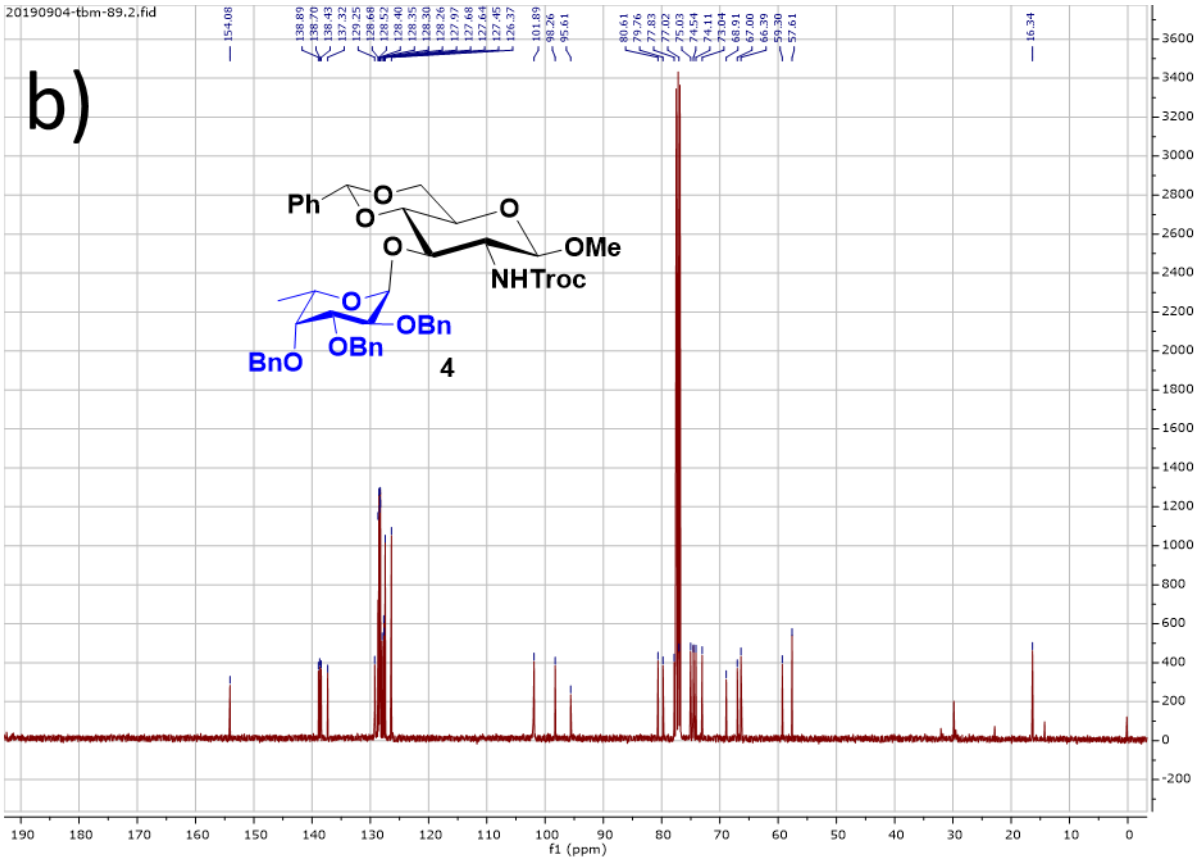

Fig. S9: NMR Spectra of Compound 4. ^{1}H **(a)** and ^{13}C **(b)** NMR spectra. (α-Isomer) ^{1}H NMR (400 MHz, Chloroform-*d*) δ 7.47 - 7.45 (m, 2H), 7.41 – 7.27 (m, 18H), 5.50 (s, 1H), 5.43 (s, 1H), 5.16 (d, *J* = 3.6 Hz, 1H), 4.92 (d, *J* = 11.5 Hz, 1H), 4.86 – 4.70 (m, 6H), 4.63 – 4.57 (m, 2H), 4.36 (dd, *J* = 10.5, 4.9 Hz, 1H), 4.26 (t, *J* = 9.6 Hz, 1H), 4.10 – 4.04 (m, 2H), 3.94 (dd, *J* = 10.2, 2.8 Hz, 1H), 3.77 (t, *J* = 10.3 Hz, 1H), 3.63 – 3.57 (m, 2H), 3.53 – 3.45 (m, 1H) 3.48 (s, 3H), 3.29 (q, *J* = 8.4 Hz, 1H), 0.78 (d, *J* = 6.4 Hz, 3H). 13C NMR (100 MHz, Chloroform-*d*) δ 154.1, 138.9, 138.7, 138.4, 137.3, 129.3, 128.7, 128.5, 128.4, 128.4, 128.3, 128.3, 128.0, 127.7, 127.6, 127.5, 126.4, 101.9, 98.3, 95.6, 80.6, 79.8, 77.8, 77.0, 75.0, 74.5, 74.1, 73.0, 68.9, 67.0, 66.4 , 59.3, 57.6, 16.3. HRMS (ESI) calcd. for $C_{44}H_{48}Cl_3NO_{11}$ $[M + H]^+$ 872.2311, found 872.2315.

Synthesis and NMR Spectra of Compound 5

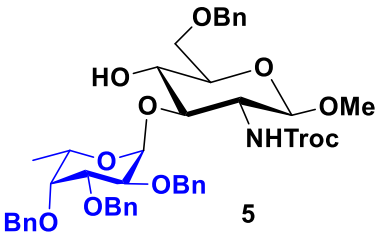

A solution of **4** (500 mg, 0.572 mmol, 1.0 equiv) and activated 4Å powdered molecular sieves (0.6 g) in anhydrous dichloromethane (10 ml) was stirred for 1 hour at room temperature under N_2 atmosphere, and then cooled to -78 °C followed by drop wise addition of Et_3SiH (100.6 μl, 0.630 mmol, 1.1 equiv) and then TfOH (56 μl, 0.630 mmol, 1.1 equiv). The reaction mixture was stirred at -78 °C for 3 hours until the disappearance of the starting material on TLC, then quenched with triethylamine and warmed to room temperature. The mixture was diluted with dichloromethane, filtered through celite, dried over Na_2SO_4, and concentrated under reduced pressure. The residue was purified by column chromatography on silica gel to afford the compound **5** (407 mg, 81 %).

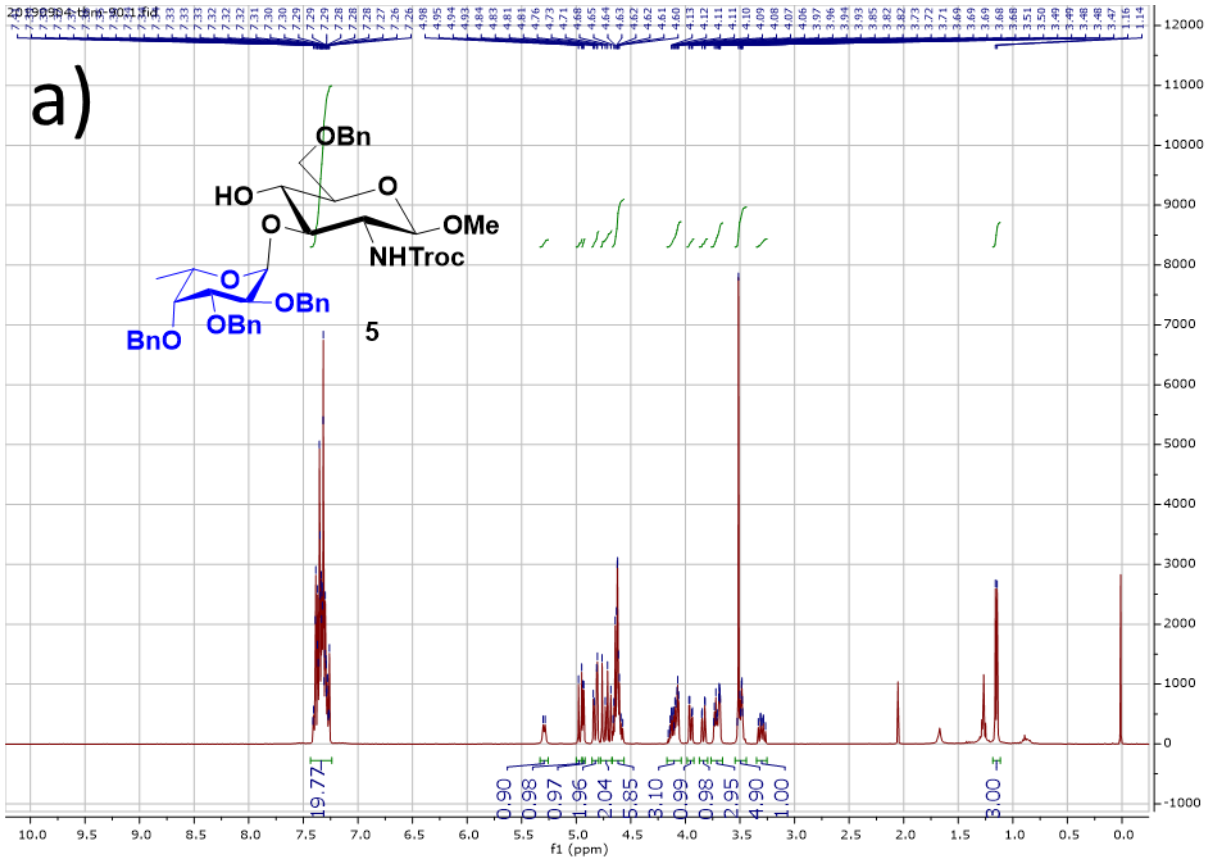

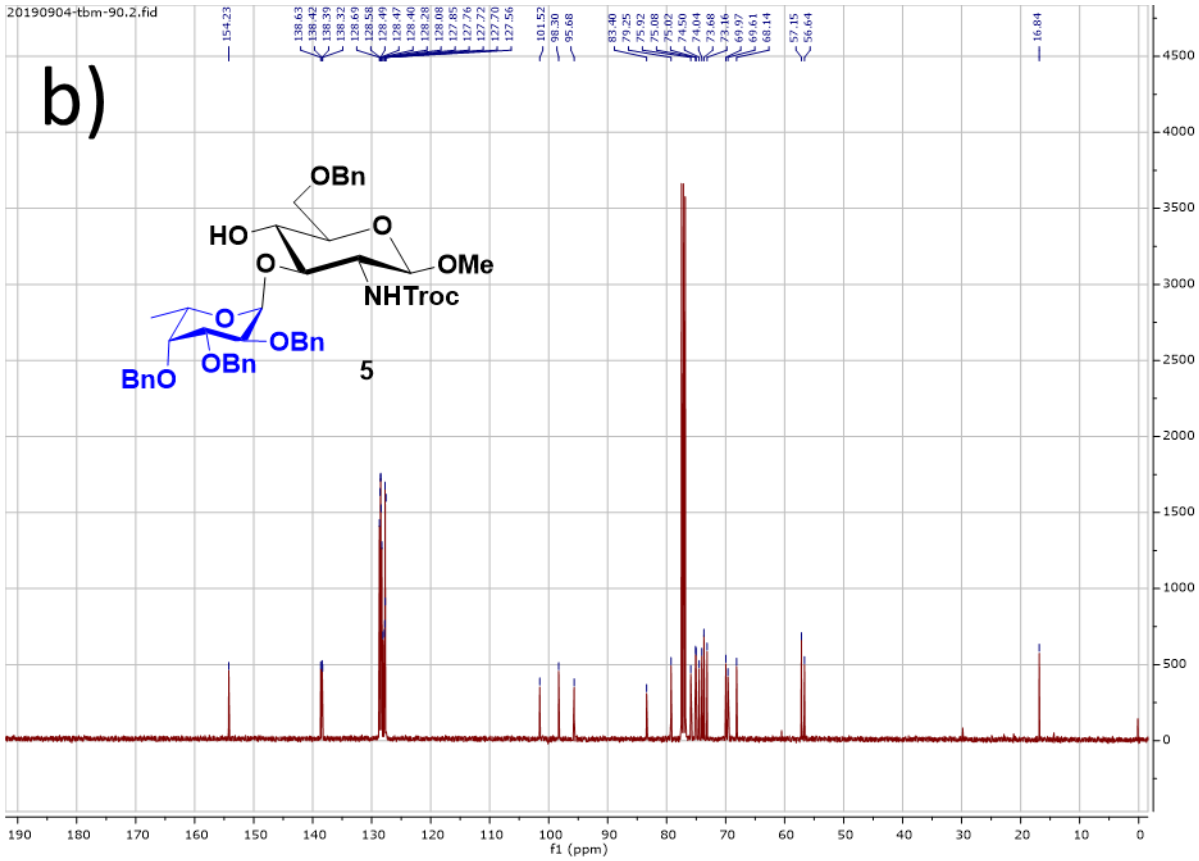

Fig. S10: NMR Spectra of Compound 5. ^{1}H **(a)** and ^{13}C **(b)** NMR spectra. ^{1}H NMR (400 MHz, Chloroform-*d*) δ 7.43 – 7.26 (m, 20H), 5.29 (d, *J* = 7.3 Hz, 1H), 4.96 (d, *J* = 11.4 Hz, 1H), 4.93 (d, *J* = 3.7 Hz, 1H), 4.82 (dd, *J* = 11.8, 3.4 Hz, 2H), 4.76 – 4.68 (m, 2H), 4.66 – 4.57 (m, 6H), 4.16 – 4.04 (m, 3H), 3.95 (dd, *J* = 10.1, 2.7 Hz, 1H), 3.83 (dd, *J* = 10.8, 1.8 Hz, 1H), 3.74 – 3.68 (m, 3H), 3.52 – 3.47 (m, 2H), 3.51 (s, 3H), 3.33 – 3.27 (m, 1H), 1.15 (d, *J* = 6.5 Hz, 3H). ^{13}C NMR (101 MHz, Chloroform-*d*) δ 154.2, 138.6, 138.4, 138.4, 138.3, 128.7, 128.6, 128.5, 128.5, 128.4, 128.3, 128.1, 127.9, 127.8, 127.7, 127.7, 127.6, 101.5, 98.3, 95.7, 83.4, 79.3, 75.9, 75.1, 75.0, 74.5, 74.0, 73.7, 73.2, 70.0, 69.6, 68.1, 57.2, 56.6, 16.8. HRMS (ESI) calcd. for $C_{44}H_{50}Cl_3NO_{11}$ $[M + H]^+$ 874.2528, found 874.2532.

Synthesis and NMR Spectra of Compound 7

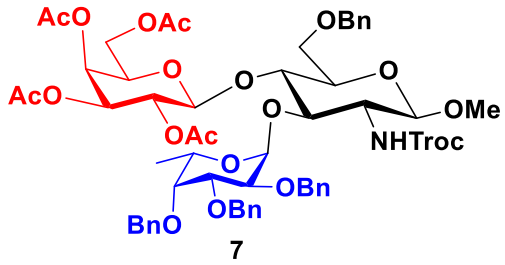

7

A solution of **5** (200 mg, 0.229 mmol, 1.0 equiv), galactose donor **6** (0.135 mg, 0.274 mmol, 1.2 equiv), and activated 4Å powdered molecular sieves (0.4 g) in anhydrous dichloromethane (5 ml) was stirred for 2 hours at room temperature under N_2 atmosphere, and then cooled to -40 °C followed by addition of TMSOTf (17 *µl*, 0.091 mmol, 0.4 equiv). The reaction mixture was stirred at -40 °C for 25 min until the disappearance of the donor on TLC, then quenched with triethylamine and warmed to room temperature. The mixture was diluted with dichloromethane, filtered through celite, dried over Na_2SO_4, and concentrated under reduced pressure. The residue was purified by column chromatography on silica gel to afford the compound **7** (202 mg, 73 %).

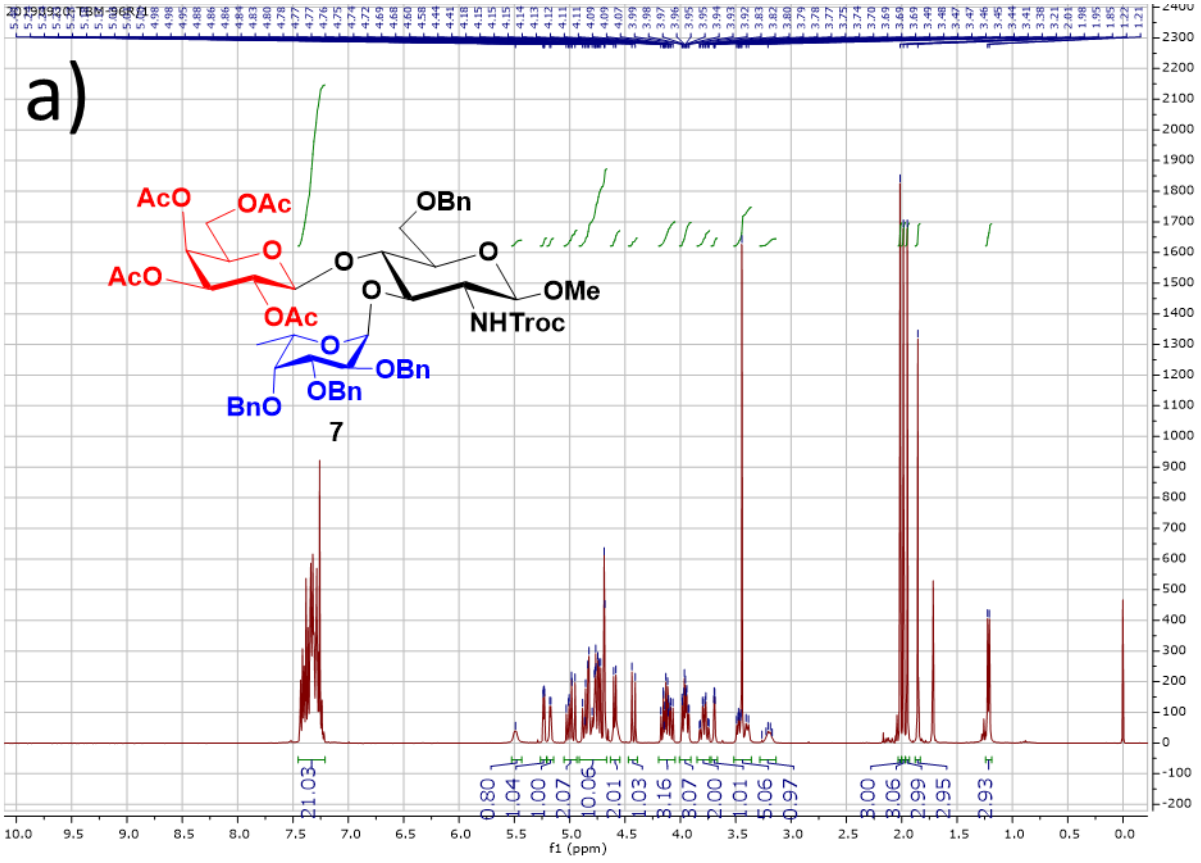

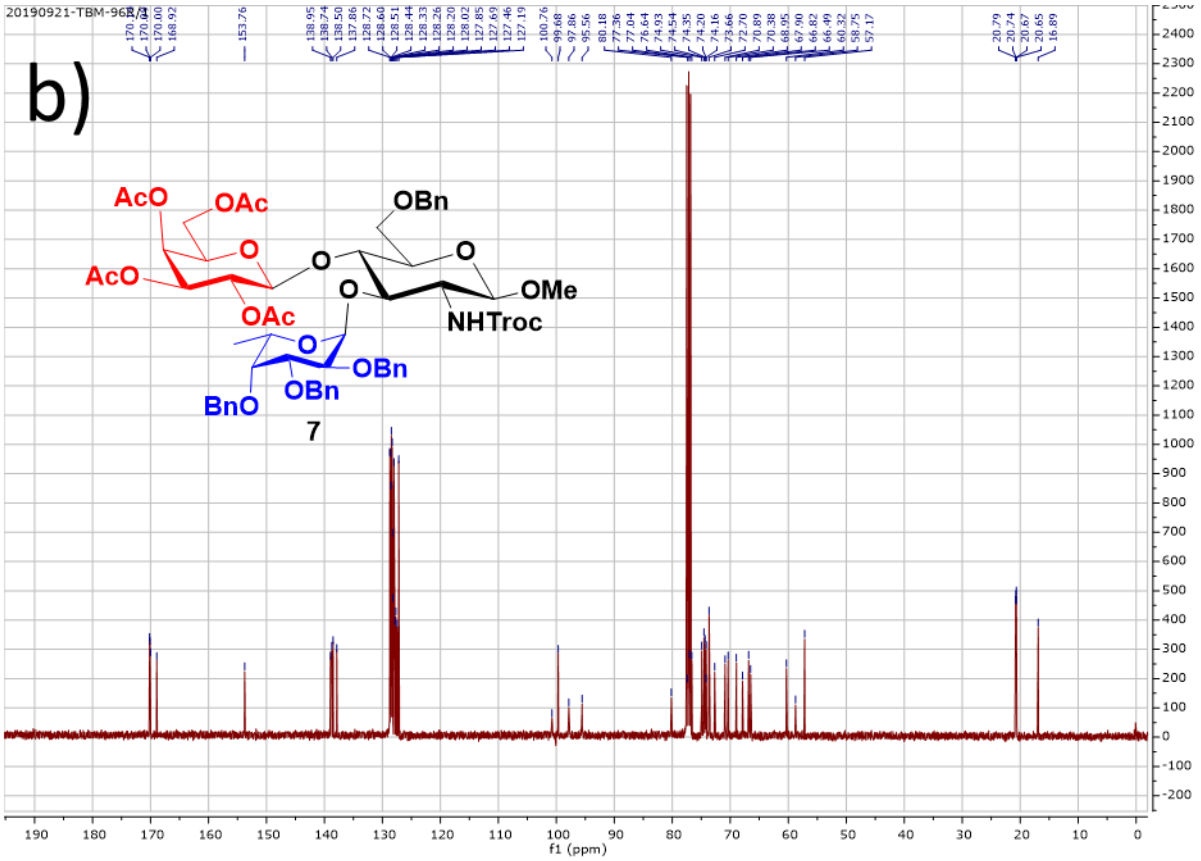

Fig. S11: NMR Spectra of Compound 7. ^{1}H **(a)** and ^{13}C **(b)** NMR spectra. (β-Isomer) ^{1}H NMR (400 MHz, Chloroform-*d*) δ 7.44 – 7.22 (m, 20H), 5.49 (s, 1H), 5.23 (dd, *J* = 3.6, 1.2 Hz, 1H), 5.17 (d, *J* = 3.8 Hz, 1H), 5.03 – 4.95 (m, 2H), 4.88 – 4.68 (m, 10H), 4.59 (d, *J* = 8.2 Hz, 2H), 4.42 (d, *J* = 12.0 Hz, 1H), 4.18 – 4.07 (m, 3H), 3.99 – 3.92 (m, 3H), 3.8 – 3.74 m, 2H), 3.69 (d, *J* = 2.7, 1H), 3.49 – 3.38 (m, 2H), 3.44 (s, 3H) 3.26 – 3.17 (m, 2H), 2.01 (s, 3H), 1.98 (s, 3H), 1.95 (s, 3H), 1.85 (s, 3H), 1.22 (d, *J* = 6.5 Hz, 3H). ^{13}C NMR (100 MHz, Chloroform-*d*) δ 170.1, 170.1, 170.0, 168.9, 153.8, 139.0, 138.7, 138.5, 137.9, 128.7, 128.6, 128.5, 128.4, 128.3, 128.3, 128.2, 128.0, 127.9, 127.7, 127.5, 127.2, 100.8, 99.7, 97.9, 95.6, 80.2, 77.4, 77.0, 76.6, 74.9, 74.5, 74.4, 74.2, 74.2, 73.7, 72.7, 70.9, 70.4, 69.0 , 67.9, 66.8, 66.5, 60.3, 58.8, 57.2, 20.8, 20.7, 20.7, 20.7, 16.9. HRMS (ESI) calcd. for $C_{58}H_{68}Cl_3NO_{20}$ $[M + H]^+$ 1204.3479, found 1204.3475.

Synthesis and NMR Spectra of Compound 8 (Lewis^X)

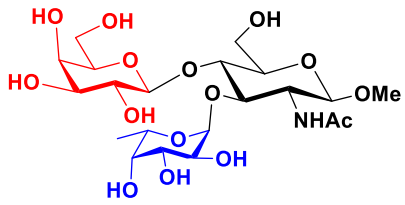

8 Lewis X

To a stirred solution of **7** (180 mg, 0.149 mmol, 1.0 equiv), in THF/H_2O (4 ml, 2:1) was added LiOH.H_2O (125 mg, 2.99 mmol, 20 equiv), and heated at 80 °C for 12 hours. Then the reaction was neutralised with IR-120H+ resin to pH-7, diluted in methanol, filtered and concentrated under reduced pressure. This residue was dissolved in methanol (3 ml), added Et_3N (208 *µl*, 1.49 mmol, 10 equiv), cooled to 0°C and then added Ac_2O (71 *µl*, 0.747 mmol, 5 equiv) and stirred for 2 hours. The reaction mixture was concentrated under reduced pressure, then dissolved in DCM and washed with 10% HCl. Then this DCM layer was concentrated under reduced pressure. This residue was then dissolved in MeOH (2 ml) and 10% Pd–C (20 mg) was added to this solution. The reaction mixture was stirred for 2 days at room temperature until completion of the reaction. Then the reaction mixture was diluted with methanol and filtered through celite, concentrated under reduced pressure and purified by reverse-phase column chromatography (Bond Elu-C18) to afford the compound **8** as white solid after lyophilisation (20 mg, 44 %).

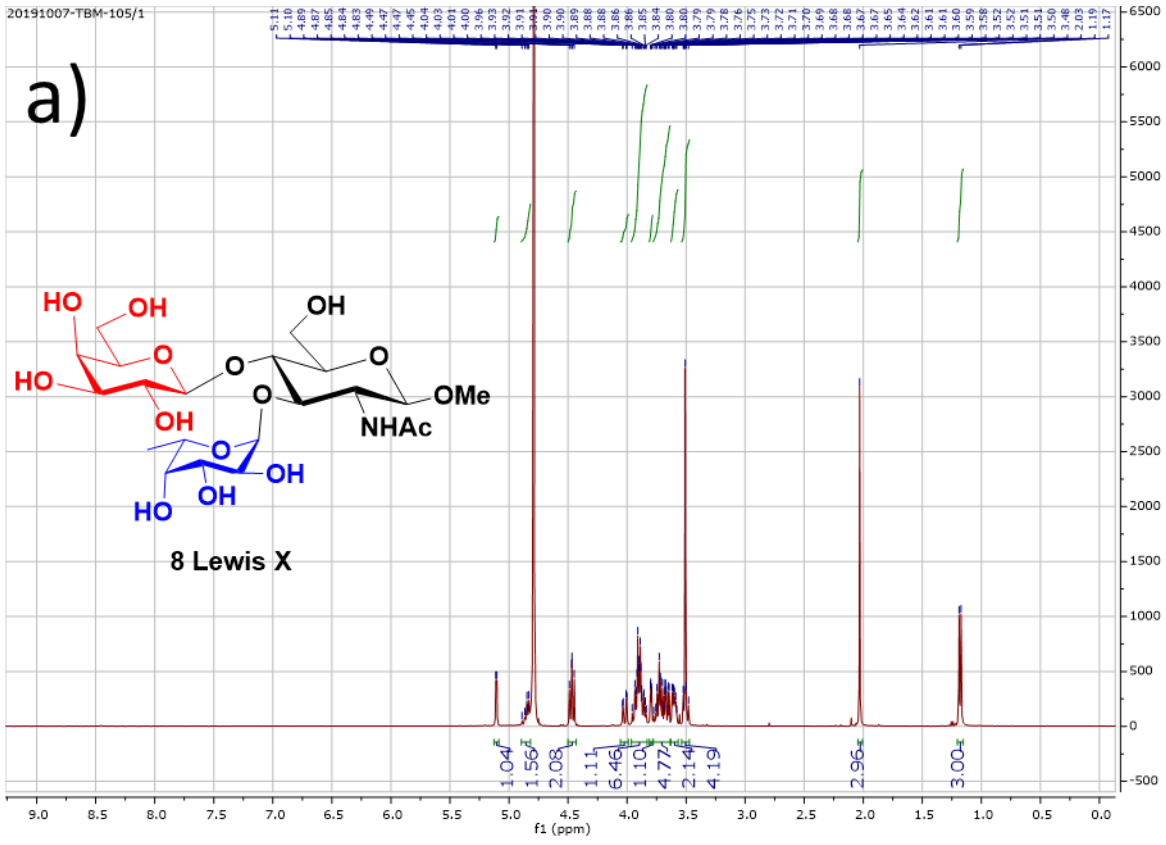

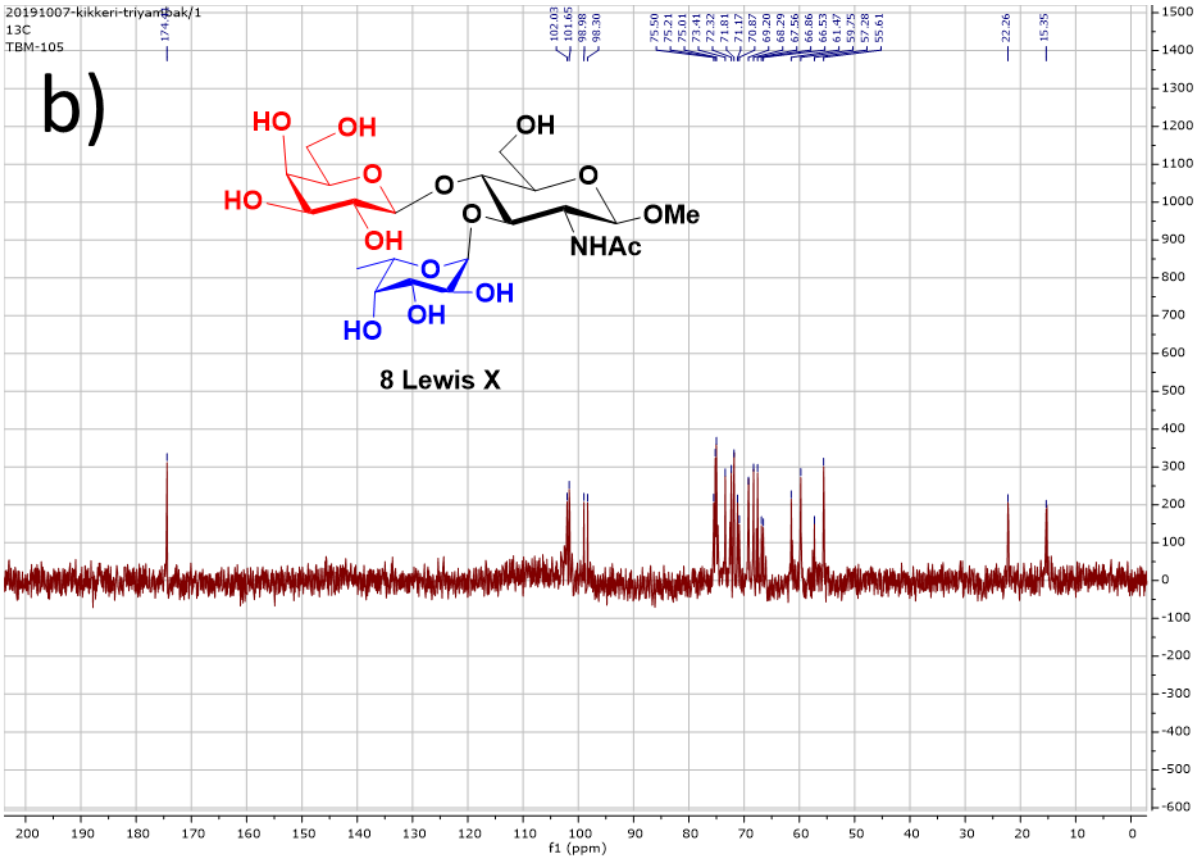

Fig. S12: NMR Spectra of Compound 8 (Lewis^x). ^{1}H **(a)** and ^{13}C **(b)** NMR spectra. ^{1}H NMR (400 MHz, Deuterium Oxide) δ 5.11 (d, *J* = 4.0 Hz, 1H), 4.89 – 4.83 (m, 2H), 4.49 – 4.45 (m, 2H), 4.02 (dd, *J* = 12.3, 2.4 Hz, 1H), 3.96 – 3.88 (m, 6H), 3.80 (dd, *J* = 3.3, 1.1 Hz, 1H), 3.78 – 3.64 (m, 5H), 3.62 – 3.58 (m, 2H), 3.52 – 3.48 (m, 1H) 3.51 (s, 3H), 2.03 (s, 3H), 1.18 (d, *J* = 6.6 Hz, 3H). ^{13}C NMR (126 MHz, Deuterium Oxide) δ 174.4, 102.0, 101.7, 99.0, 98.3, 75.5, 75.2, 75.0, 73.4, 72.3, 71.8, 71.2, 70.9, 69.2, 68.3, 67.6, 66.9, 66.5, 61.5, 59.8, 57.3, 55.6, 22.3, 15.4 . HRMS (ESI) calcd. for $C_{21}H_{37}NO_{15}$ $[M + H]^+$ 544.2241, found 544.2239.

S6. Supplementary Information References

Afsahi, S., Lerner, M. B., Goldstein, J. M., Lee, J., Tang, X., Bagarozzi, D. A., Pan, D., Locascio, L., Walker, A., Barron, F. and Goldsmith, B. R. 2018. Biosensors and Bioelectronics 100, 85-88.

Barondes, S. H., Cooper, D. N. W., Gitt, M. A. and Leffler, H. 1994. The Journal of Biological Chemistry 269, 20807-20810.

Çakıroğlu, B., Demirci, Y. C., Gökgöz, E. and Özacar, M. 2019. Sensors and Actuators B: Chemical 282, 282-289.

Campos, R., Machado, G., Cerqueira, M. F., Borme, J. and Alpuim, P. 2018. Microelectronic Engineering 189, 85-90.

Danielson, E., Dhamodharan, V., Porkovich, A., Kumar, P., Jian, N., Ziadi, Z., Grammatikopoulos, P., Sontakke, V. A., Yokobayashi, Y. and Sowwan, M. 2019. Scientific Reports 9, 17370.

Datta, A., Porkovich, A. J., Kumar, P., Nikoulis, G., Kioseoglou, J., Sasaki, T., Steinhauer, S., Grammatikopoulos, P. and Sowwan, M. 2019. The Journal of Physical Chemistry C 123, 26124-26135.

Gasteiger, E., Hoogland, C., Gattiker, A., Duvaud, S., Wilkins, M. R., Appel, R. D. and Bairoch, A. (2005). Protein Identification and Analysis Tools on the ExPASy Server. The Proteomics Protocols Handbook. J. M. Walker, Humana Press**:** 571-607.

Graf, D., Molitor, F., Ensslin, K., Stampfer, C., Jungen, A., Hierold, C. and Wirtz, L. 2007. Nano Letters 7, 238-242.

Grammatikopoulos, P., Steinhauer, S., Vernieres, J., Singh, V. and Sowwan, M. 2016. Advances in Physics: X 1, 81-100.

Han, B., Han, Z., Qin, J., Wang, Y. and Zhao, Z. 2019. Talanta 192, 1-5.

Hefti, M. H., Van Vugt-Van der Toorn, C. J. G., Dixon, R. and Vervoort, J. 2001. Analytical Biochemistry 295, 180-185.

Johannes, L., Jacob, R. and Leffler, H. 2018. Journal of Cell Science 131, jcs208884.

Kasai, K.-i. and Hirabayashi, J. 1996. The Journal of Biochemistry 119, 1-8.

Lis, H. and Sharon, N. 1998. Chemical Reviews 98, 637-674.

Liu, F.-T. and Rabinovich, G. A. 2010. Annals of the New York Academy of Sciences 1183, 158-182.

Lopez, F., Ma, S., Ludwig, R., Schuhmann, W. and Ruff, A. 2017. Electroanalysis 29, 154-161.

MacKinnon, A. C., Farnworth, S. L., Hodkinson, P. S., Henderson, N. C., Atkinson, K. M., Leffler, H., Nilsson, U. J., Haslett, C., Forbes, S. J. and Sethi, T. 2008. The Journal of Immunology 180, 2650.

Massa, S. M., Cooper, D. N. W., Leffler, H. and Barondes, S. H. 1993. Biochemistry 32, 260-267.

Nguyen, B. H., Nguyen, B. T., Van Vu, H., Van Nguyen, C., Nguyen, D. T., Nguyen, L. T., Vu, T. T. and Tran, L. D. 2016. Current Applied Physics 16, 135-140.

No, Y.-S., Choi, H. K., Kim, J.-S., Kim, H., Yu, Y.-J., Choi, C.-G. and Choi, J. S. 2018. Scientific Reports 8, 571.

Porkovich, A. J., Ziadi, Z., Kumar, P., Kioseoglou, J., Jian, N., Weng, L., Steinhauer, S., Vernieres, J., Grammatikopoulos, P. and Sowwan, M. 2019. ACS Nano 13, 12425-12437.

Rajendran, V. and Irudayaraj, J. 2002. Journal of Dairy Science 85, 1357-1361.

Roscher, S., Hoffmann, R. and Ambacher, O. 2019. Analytical Methods 11, 1224-1228.

Shivayogimath, A., Whelan, P. R., Mackenzie, D. M. A., Luo, B., Huang, D., Luo, D., Wang, M., Gammelgaard, L., Shi, H., Ruoff, R. S., Bøggild, P. and Booth, T. J. 2019. Chemistry of Materials 31, 2328-2336.

Steinhauer, S., Singh, V., Cassidy, C., Gspan, C., Grogger, W., Sowwan, M. and Köck, A. 2015. Nanotechnology 26, 175502.

Tasca, F., Ludwig, R., Gorton, L. and Antiochia, R. 2013. Sensors and Actuators B: Chemical 177, 64-69.

Vernieres, J., Steinhauer, S., Zhao, J., Grammatikopoulos, P., Ferrando, R., Nordlund, K., Djurabekova, F. and Sowwan, M. 2019. Advanced Science 6, 1900447.

Wu, R., Gan, L., Ou, X., Zhang, Q. and Luo, Z. 2016. Carbon 98, 138-143.

Yakovleva, M., Buzas, O., Matsumura, H., Samejima, M., Igarashi, K., Larsson, P.-O., Gorton, L. and Danielsson, B. 2012. Biosensors and Bioelectronics 31, 251-256.